The structure of the C-terminal actin-binding domain of talin

Alexandre R. Gingras, Neil Bate, Benjamin T. Goult, Larnele Hazelwood, Ilona Canestrelli, J. Günter Grossmann, HongJun Liu, Nicholas S.M. Putz, Gordon C.K.Roberts, Niels Volkmann, Dorit Hanein, Igor L. Barsukov, and David R. Critchley

SUPPLEMENTAL DATA

RESULTS

Domain boundaries of the C-terminal region of talin

Secondary structure analysis of the C-terminal actin binding domain of the talin rod (the I/LWEQ motif (Senetar et al, 2004) or THATCH domain (Brett et al, 2006)) predicts six α-helices (Figure 1A). To characterise the structure of this region, we initially compared the ^{15}N-HSQC spectra of talin 2294-2541 (Figure S1A) with that of the shorter talin 2294-2491 polypeptide (Figure S1B) lacking the last helix which is implicated in talin dimer formation (Senetar et al, 2004). Both spectra had a large number of highly dispersed cross-peaks at virtually identical positions demonstrating the presence of a similar folded domain in both polypeptides. In addition, there were a number of intense sharp resonances corresponding to unstructured regions. The spectrum of the larger fragment generally had broader resonances and also contained unresolved broad cross-peaks - no new resolved peaks were observed. It has been shown previously for both talin (Senetar et al, 2004) and HIP1R (Brett et al, 2006) that the C-terminal region is dimeric which fits with the broadening of the resonances. However, the peak broadening is not as extensive as expected from a dimer which suggests that the monomer units within the dimer retain some independent mobility. This interpretation is in agreement with the lack of significant chemical shift changes in the resonances of the folded region in the presence or absence of the last helix, indicating that there is a limited interaction between the folded core and the dimerisation domain. Detailed analysis of the [^{1}H,^{15}N]-HSQC spectra of different talin fragments provide clear evidence for such an interaction (see main text). The structures of the two domains can therefore be studied independently.

To optimise the domain boundaries, we assigned the sharp resonances in the ^{15}N-HSQC spectra of talin 2294-2491 using triple-resonance methods. These signals corresponded to residues 2294-2300 and 2478-2491 at the N- and C-termini of the domain and region 2326-2340 between the predicted helices 1 and 2. Removal of the N- and C-terminal unstructured regions improved the quality of the spectra without affecting the structure, as shown by the similarity of the chemicals shifts of talin 2294-2491 (Figure S1B) and talin 2300-2482 (Figure S1D).

The N-terminal helix of the actin binding domain has the lowest sequence homology to HIP1 and HIP1R. This region (referred to as the USH) is reported to negatively regulate the talin/actin interaction (Senetar et al, 2004) suggesting the existence of a smaller independent four-helix structural domain. The ^{15}N-HSQC spectrum of the fragment comprising this domain (residues 2334-2491) is shown in Figure S1C. The differences in the chemical shifts between the spectrum of the 5-helix talin polypeptide 2294-2491 (Figure S1B) and the 4-helix 2334-2491 polypeptide (Figure S1C) indicate significant structural rearrangements upon removal of the N-terminal helix. In addition, the spectrum of the shorter fragment contains a large numbers of severely broadened resonances indicating internal dynamics within the structure. When expressed as a His-tag polypeptide most of the 4-helix fragment accumulated in inclusion bodies, resulting in a low yield of the soluble protein. Attempts to concentrate the protein above 0.3 mM lead to precipitation. When expressed as a thioredoxin-fusion, the polypeptide remained soluble until the tag was cleaved. In contrast, no precipitation of the 5-helix fragment 2300-2482 was observed up to a concentration of 1.5 mM. These observations demonstrate that the five-helix talin polypeptide exists as a stable globular protein corresponding to the HIP1R THATCH core domain (Brett et al, 2006), and that removal of the N-terminal USH leads to destabilisation of the structure. The CD signal at 222 nm which reports on helical structure shows a sharp transition at 90ºC indicating that residues 2294-2491 form a very stable fold (data not shown).

The ^{15}N-HSQC spectrum of the talin 2481-2541 fragment which includes the dimerisation domain (Figure S3A) showed a mixture of sharp resonances with low chemical shift dispersion, corresponding to a highly mobile unstructured region, as well as more dispersed broader signals corresponding to a structured domain. The majority of the sharp signals were assigned to the N-terminal region 2481-2495. Removal of the unstructured N-terminal residues in talin 2481-2541 had very little

effect on resonances from the structured region, identifying the minimal dimerisation domain as 2494-2541 (Figure S3B). The CD spectra of the dimerisation domain showed a high content of α-helical structure. The NMR resonances of the fragment are substantially broader than expected from the molecular weight (~6kDa). Dimerisation, indicated in previous studies (Senetar et al, 2004) and confirmed here by gel filtration (data not shown) is not sufficient to explain this severe resonance broadening, and the most likely explanation is the formation of a highly anisotropic elongated dimeric structure. In summary, the initial characterisation of C-terminal actin binding site of talin by NMR demonstrates the presence of a stable globular domain (residues 2300-2482) equivalent to the core of the HIP1R THATCH domain (Brett et al, 2006) connected by a flexible linker to a helical dimerisation domain (residues 2496-2529). Removal of the dimerisation domain does not affect the structure of the core, whereas the removal of the N-terminal helix destabilises the structure.

NMR structure determination of the C-terminal actin-binding domain of talin

Despite the high stability and high quality of the NMR spectra of the talin 2300-2482 polypeptide our attempts to crystallise it failed, while the crystals of the corresponding domain from HIP1R were readily obtained (Brett et al, 2006). We have experienced similar problems with other fragments from the talin rod, and this is likely due to the surface charge distribution and/or the inherent flexibility of the loops within the helical bundles that make up the rod. The stability of the structure shown by the CD temperature profile allowed us to use higher temperatures to enhance the quality of the NMR spectra, thus facilitating structure determination. The comparison of the ^{15}N-HSQC spectra showed no structural changes up to at least 55^{o}C. As a compromise between the long-term stability and the quality of the spectra we selected 45^{o}C for NMR data collection. The resonances have been assigned by conventional triple-resonance experiments using [^{13}C,^{15}N]-labelled protein, and the solution structure has been determined using 3791 unique and 827 ambiguous distance constraints from NOEs, 290 TALOS dihedral angles constraints from ^{13}C chemical shift values and 63 hydrogen bonds involving slow-exchanging amide protons (Table SI).

Comparison of the THATCH core domain and other 5-helix bundles

The topology of the helical bundle that makes up the talin C-terminal actin binding domain differs from that of other 5-helix bundles within the talin rod (Papagrigoriou et al, 2004). In all the 5-helical bundle structures, helices 2-5 have a common topology, but sometimes can have a different handedness. Where these structures diverge most is in the location of helix α1 (Figure S2D). The five helices of the talin THATCH core domain are arranged progressively as first described for the THATCH core domain of HIP1R (Brett et al, 2006). In the THATCH core domains, helix 1 packs against helices 2 and 3, while in the left handed crossover connectivity observed for talin 482-655, helix 1 packs against helices 3 and 4 (Figure S2D). The vinculin tail shows a circular connectivity (Bakolitsa et al, 1999) (helix 1 packs against helices 2 and 5) and apolipophorin III shows a right handed crossover connectivity (Breiter et al, 1991) (helix 1 packs against helices 4 and 5).

Crystal structure determination of the talin dimerisation domain

We initially started our structural studies on the talin dimerisation domain using a C-terminal fragment (residues 2481-2541). NMR assignment of the dimerisation domain showed that the first 12 residues were unfolded as were some of the residues from the C-terminal region (Figure S3A). This N-terminal region shows low sequence conservation with HIP1R and Sla2p proteins. Therefore, a new construct was produced (residues 2494-2541) that showed improved NMR line width with few unfolded residues remaining from the C-terminus (Figure S3B). However, NMR studies on this dimerisation domain were non-trivial due to severe line broadening (see above). Fortunately, large crystals that diffracted X-rays to 2.2 Å resolution were readily obtained using sparse matrix screening, and the crystal structure was determined using single wavelength anomalous diffraction (SAD) from a selenomethionine derivative (Table SII). The solvent-flattened map shown in Figure S4A was easily interpretable, and clearly showed one dimer in the asymmetric unit.

Analysis of the talin THATCH domain by gel filtration

Analytical gel filtration studies on the talin THATCH domain (residues 2300-2541) indicate the presence of a dimeric particle in solution (Figure S6). The talin 2300-2541 polypeptide shows a shorter retention time than the construct (2300-2482)

lacking the dimerisation domain, although each migrated as a single peak (Figure S6). The calculated molecular mass of the dimeric polypeptide is 52 kDa, while that estimated from gel filtration is 63 kDa, consistent with the large R_g observed by SAXS. The monomeric mutants (Figure S6) also show a larger molecular mass by gel filtration (52 kDa) than the predicted mass of 26 kDa. These observations suggest that the dimerisation domain protrudes from the core 5-helix bundle and that (i) the dimeric polypeptide forms an extended dimer and (ii) the monomeric mutants have an increased apparent molecular mass due to the elongated shape of the 5-helix bundle and because the dimerisation helix (~60 residues) is unfolded.

MATERIALS AND METHODS

NMR spectroscopy

Slowly exchanging H^N protons were identified from the [^{1}H, ^{15}N]-HSQC spectrum collected immediately after redissolving lyophilised protein in ^2H_2O, and also from the temperature dependence of their chemical shifts.

NMR structure calculation

Distance restraints were obtained from the following experiments: 4D ^{13}C-edited HMQC-NOESY-HSQC in H2O (800MHz, 100 ms), 3D ^{15}N-edited NOESY-HSQC (800 MHz, 100 ms), ^{13}C-edited NOESY-HSQC in H_2O (800 MHz, 100 ms), and 2D NOESY in ^2H_2O and H_2O (600 MHz, 100 ms). All NOESY peaks were picked using Analysis and noise and artefact peaks were removed manually. Crosspeak intensities were used to evaluate target distances. Initial models were generated with CYANA using the CANDID (Herrmann et al, 2002) method for NOESY crosspeak assignment and calibration. These models were used as initial structures in structure calculation by ARIA (Linge et al, 2001). The acceptance tolerances in the standard protocol of ARIA 1.2 were modified to set violation tolerances to 5.0, 2.0, 1.0, 0.5, 2.0, 0.5, and 0.1 Å for iterations 2-8, respectively, with iteration 1 containing the initial models. Crosspeaks rejected by ARIA were checked manually and, if found reliable, added to the calculation. One hundred structures were calculated at each iteration, the 40 lowest energy retained and 20 used for final restraint analysis. The 30 lowest energy structures from iteration 8 were further refined in the presence of explicit water molecules.

X-ray crystallography

Data sets were indexed and reduced with XDS (Kabsch, 1993). The phase problem was solved by SAD using peak data collected at λ= 0.931. Positions of 2 of the 4 selenium atoms were found, phases were calculated to 2.3 Å resolution and an initial model was built containing 58 out of 65 amino acids present in the final model using SOLVE/RESOLVE (Terwilliger & Berendzen, 1999) (www.solve.lanl.gov). The map was of good quality (Figure S4A) and the model was improved using manual building with Coot (Emsley & Cowtan, 2004) and maximum likelihood refinement using Refmac5 (Murshudov et al, 1997). Phase extension to 2.2Å with a new dataset was carried out.

Docking of atomic models into SAXS envelopes and variance analysis

Gasbor models were converted into electron density assuming a Gaussian density distribution for each pseudo atom (each representing a residue or a water molecule). The width of the Gaussian was determined by (i) rotationally averaging the contributing atoms in a residue (Debye, 1915); (ii) fitting a single Gaussian (Guo et al, 1999); and (iii) generating a weighted average using the amino-acids content of the construct. Water molecules were approximated using a Gaussian fitted to the scattering curve of an oxygen atom.

Gel filtration

Analytical gel filtration chromatography of recombinant talin polypeptides was performed using Superdex-200 (10/300) (Amersham Biosciences) at room temperature. The column was pre-equilibrated and run in 20mM Tris pH 8.0, 150mM NaCl and 2mM DTT at a flow rate of 0.8 ml/min.

Sequence conservation

The pdb file for talin 2300-2482 was submitted to the ConSurf server (http://consurf.tau.ac.il/), which maps conservation scores onto surface residues. The results shown in Figure 2B were visualised using the CCP4MG program by colouring scores of 9 in magenta, 7-8 in yellow, and all others in white (9 - conserved, 1 - variable). The ConSurf alignment for the talin 2300-2482 contained the following sequences; P26039, TLN1_MOUSE; Q9Y490, TLN1_HUMAN; Q9Y4G6,

TLN2_HUMAN; P54939, TLN1_CHICK; Q71LX4, TLN2_MOUSE; Q02328, SLAP2_CAEEL; Q9P6L5, SLA2_SCHPO; O00291, HIP1_HUMAN; P54633, TALA_DICDI; O75146, HIP1R_HUMAN; Q9JKY5, HIP1R_MOUSE; and P33338, SLA2_YEAST.

For talin 2494-2541 the sequences were aligned using ClustalW and the conservation index is shown in Figure 3D per residue. The conserved residues shown in Figure 3C were visualised using the CCP4MG program by colouring invariant residues in magenta (100% conserved), and all the similar residues in yellow. The following sequences were used; P26039, TLN1_MOUSE; Q9Y490, TLN1_HUMAN; Q9Y4G6, TLN2_HUMAN; P54939, TLN1_CHICK; Q71LX4, SLAP2_CAEEL; Q9P6L5, SLA2_SCHPO; O00291, HIP1_HUMAN; P54633, TALA_DICDI; O75146, HIP1R_HUMAN; P33338, SLA2_YEAST; XP_896942, TLN2_MOUSE; and BAC97992, HIP1R_MOUSE.

FIGURES

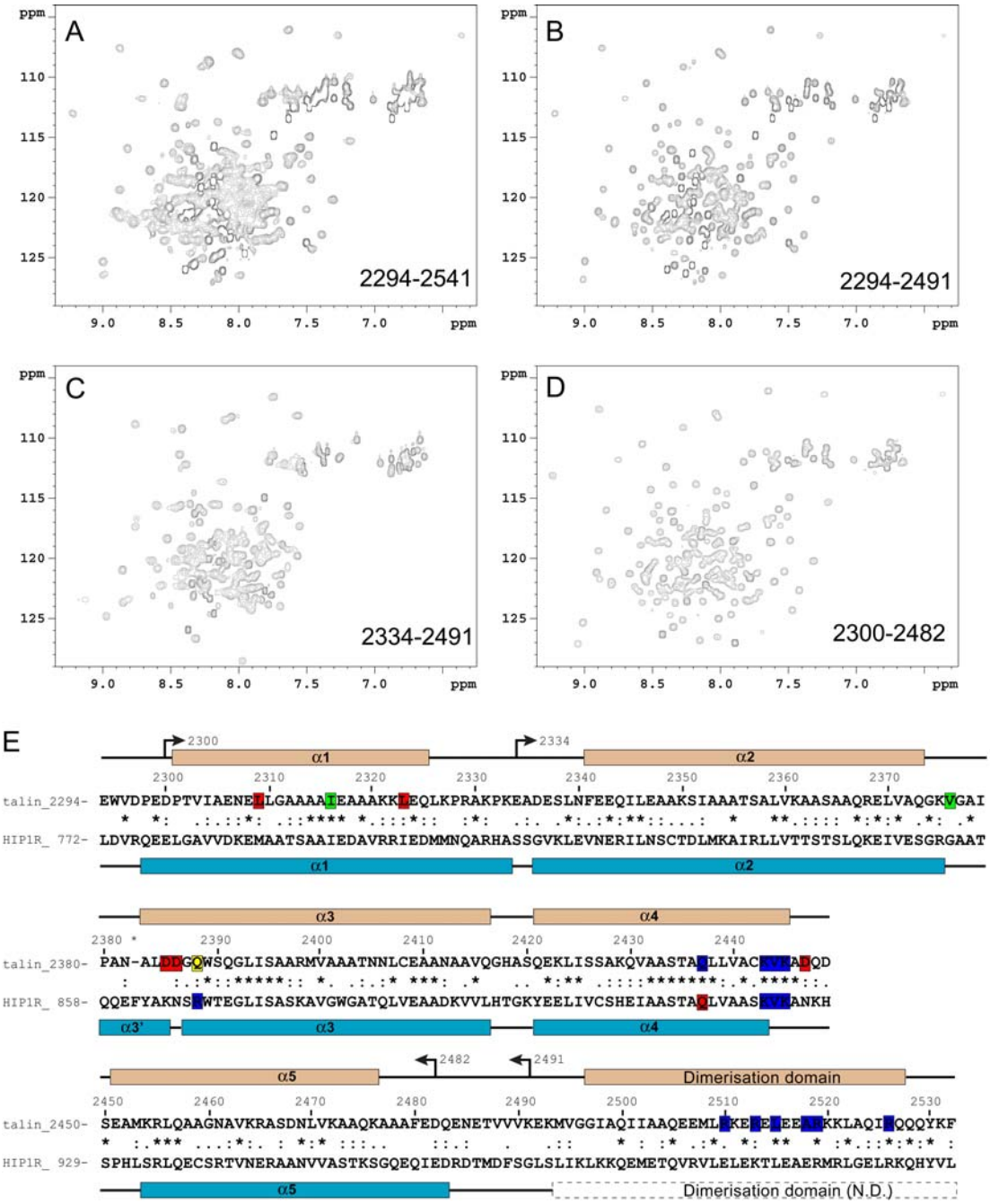

Figure S1 NMR spectra and boundaries of the C-terminal actin-binding domain in talin (the THATCH domain). (A-D) NMR ^{15}N-HSQC of talin polypeptides; (A) 2294-2541, (B) 2300-2491, (C) 2334-2491, and (D) 2300-2482. (E) Sequence alignment of mouse talin1 with the human HIP1R THATCH domain using ClustalW. Numbering is from mouse talin (P26039). Symbols denote the degree of conservation: (*) identical; (:) conserved substitutions; (.) semi-conserved substitutions. The predicted secondary structure of the mouse talin and the human HIP1R THATCH core is shown above and below the alignment respectively - the position of the putative dimerisation domain is also indicated. N.D. - structure Not Determined. Arrows indicate the boundaries of the constructs used in NMR experiments.

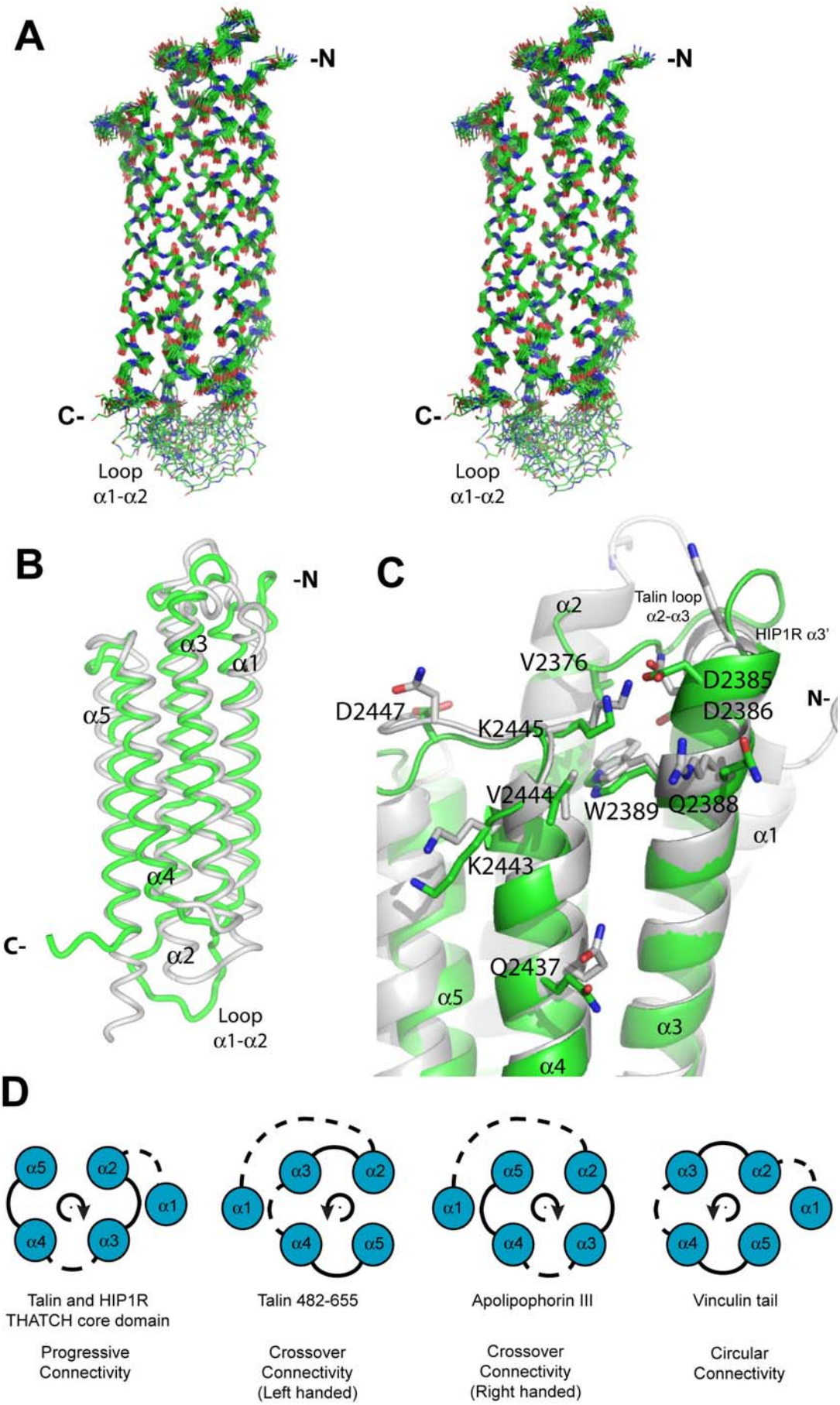
A
-N
C-
Loop
α1-α2
-N
C-
Loop
α1-α2
B
-N
α3
α1
α5
α4
C-
α2
Loop
α1-α2
C
α2
Talin loop
α2-α3
HIP1R α3'
V2376
D2385
D2386
N-
D2447
K2445
V2444
W2389
Q2388
α1
K2443
Q2437
α5
α3
α4
D
α5
α2
α1
α4
α3
Talin and HIP1R
THATCH core domain
Progressive
Connectivity
α3
α2
α1
α4
α5
Talin 482-655
Crossover
Connectivity
(Left handed)
α5
α2
α1
α4
α3
Apolipophorin III
Crossover
Connectivity
(Right handed)
α3
α2
α1
α4
α5
Vinculin tail
Circular
Connectivity

Figure S2 Solution structure of the talin C-terminal actin-binding domain (residues 2300-2482). (A) Stereoview of the superposition (using backbone atoms) of the 20 lowest energy structures consistent with the NMR data. Only the structural core region (residues 2299-2479) is shown, not the short disordered N- and C-termini. (B,C) Optimal overlay of the structure of the C-terminal actin-binding domain of talin (green) with the highly homologous HIP1R THATCH core domain (light grey, PDB entry 1R0D). (B) Optimal overlay showing the overall superimposition of both structures (r.m.s. deviation of 4.77 Å for mainchain atoms). (C) Optimal overlay showing the similarity of the predicted actin-binding interface of both proteins (35% sequence identity for the THATCH core domain). (D) Topology diagram of 5-helix bundles showing the organisation of the helices. The 5 helices of the talin THATCH core are assembled progressively as first described in (Brett et al, 2006), in contrast to the circular connectivity of vinculin tail and crossover connectivity of the talin 482-655 domain and apolipophorin III. Solid and dashed lines represent connecting loops on opposite ends of the helices. Talin 482-655 5-helix bundle (PDB endtry 1SJ7), talin C-terminal actin-binding THATCH core domain (PDB entry 2DQD), Apolipophorin III (PDB entry 1AEP), and vinculin tail (PDB entry 1QKR).

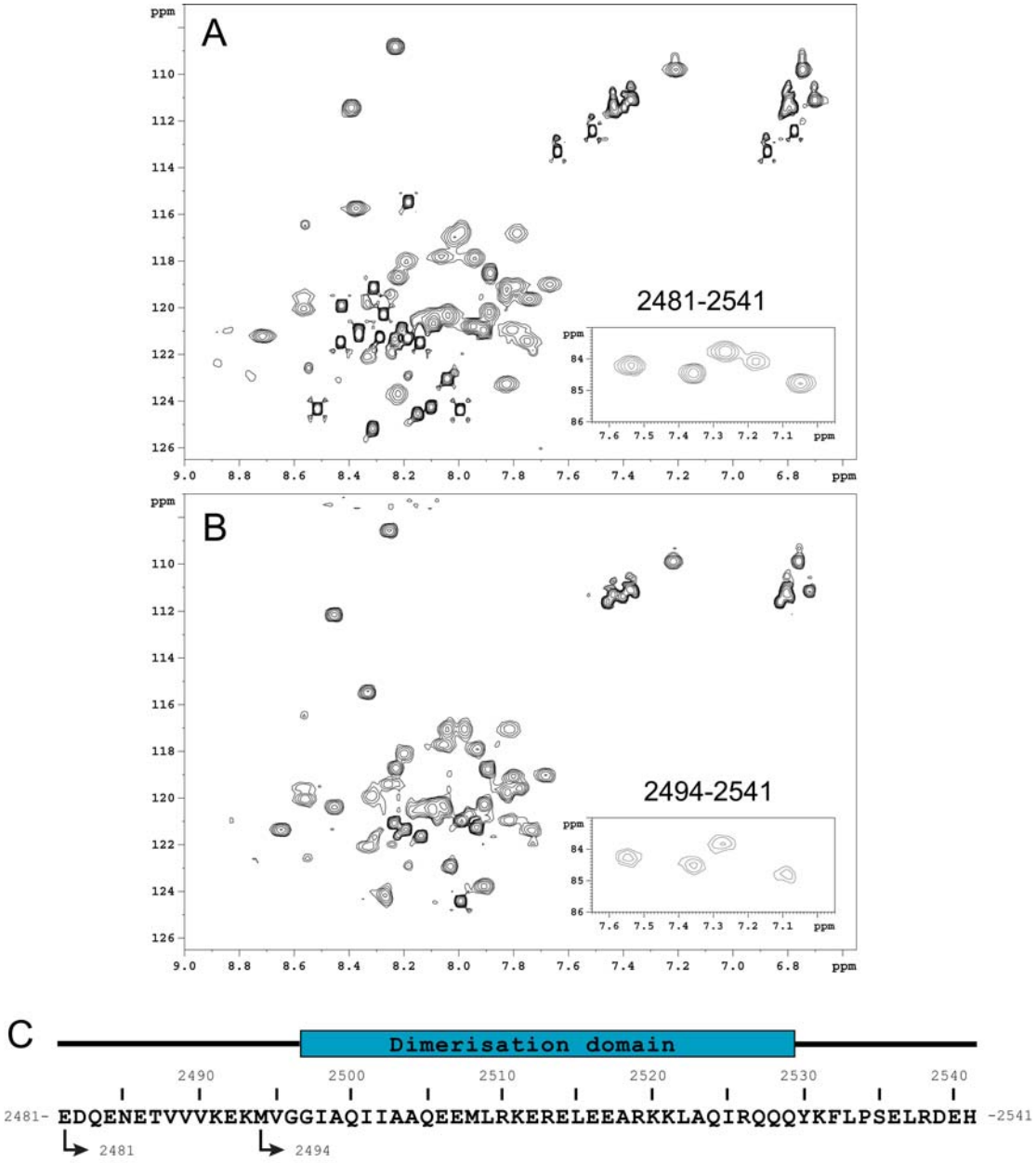

Figure S3 NMR spectra of talin dimerisation domain. (A) ^{15}N-HSQC NMR spectrum of talin 2481-2541. (B) ^{15}N-HSQC NMR spectrum of talin 2494-2541. (C) Primary sequence and secondary structure of the talin C-terminal helix. Arrows indicate the boundaries of the above talin constructs.

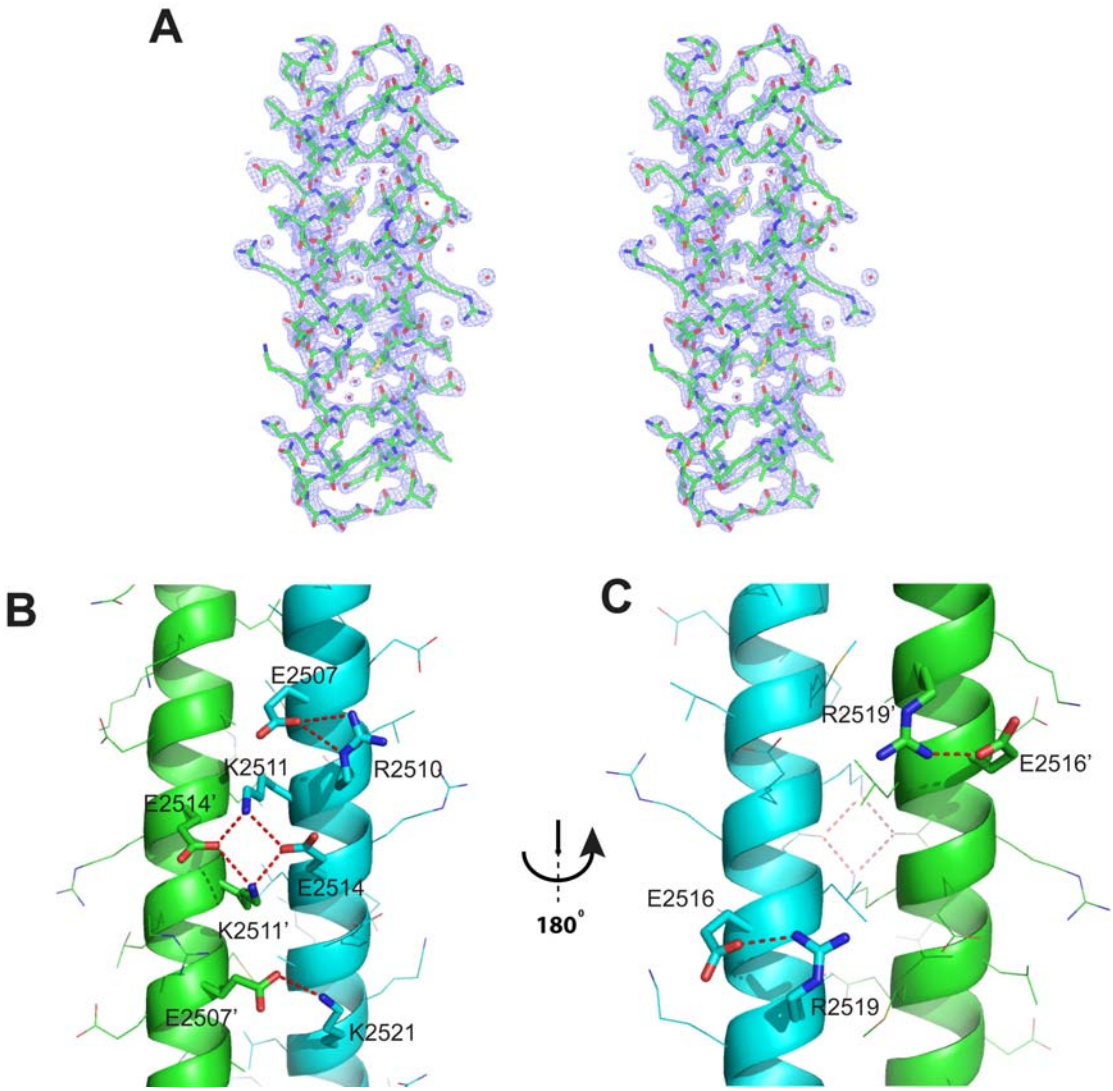

Figure S4 Electron density map of the talin dimerisation domain. (A) Stereo view of the initial SOLVE electron density map (contoured at 1.0 σ) of the talin dimerisation domain superimposed with the final model. (B, C) Close view of the salt bridges observed on the dimerisation domain surface.

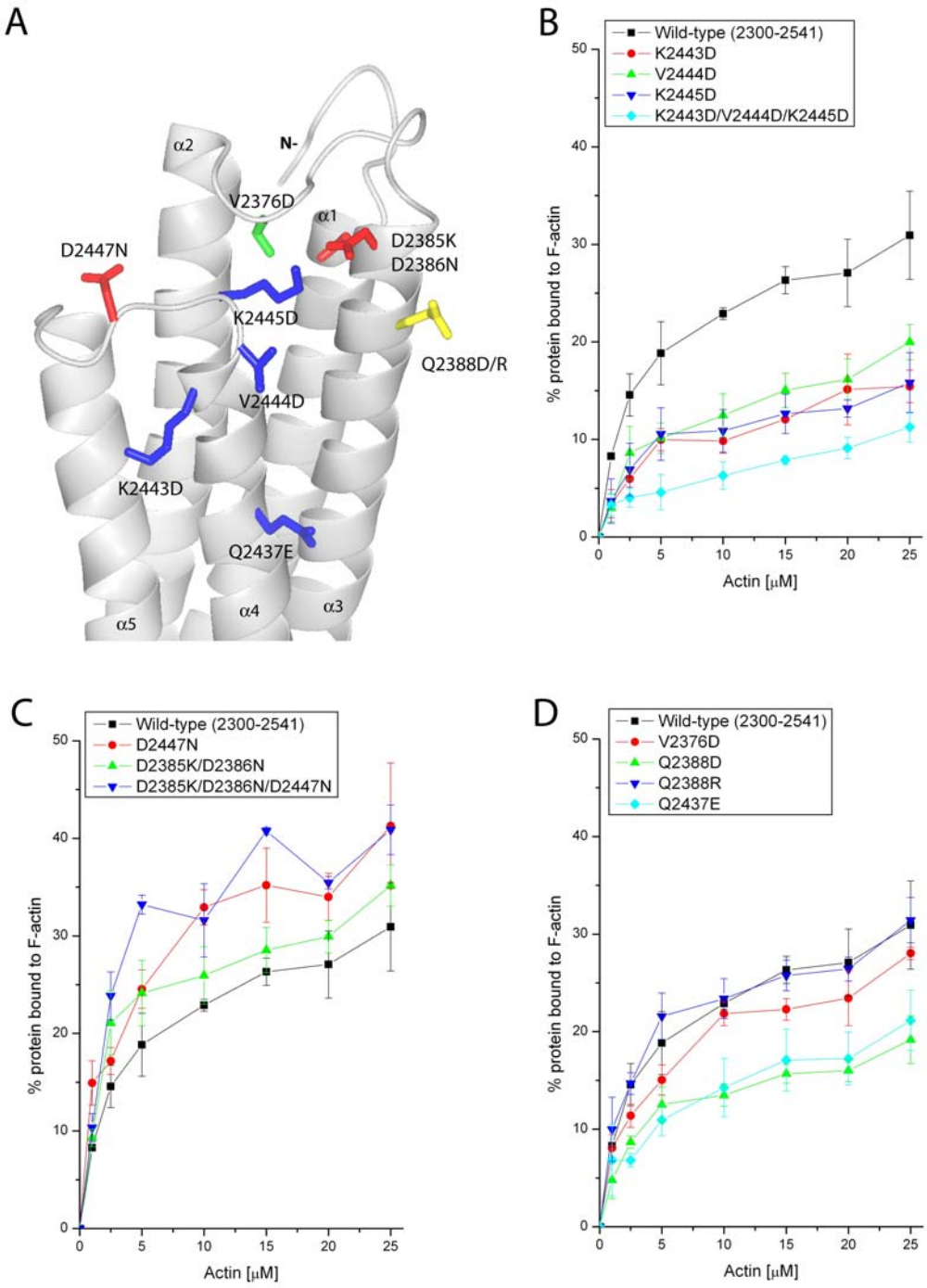

Figure S5 The actin-binding surface on the 5-helix bundle at the core of the C-terminal actin-binding domain of talin. (A) Ribbon diagram highlighting the residues targeted by mutagenesis. Residues are colour coded according to the effects of the mutation on actin binding compared to wild-type: Red - increase in binding; Green - no change; Blue - decrease in binding. Residue Q2388 is shown in yellow. (B,C,D) Quantitative analysis of the effects of the mutations on F-actin binding (means of three independent experiments). Bars represent standard deviations. Actin-binding was quantified by measuring the amount of the talin polypeptide cosedimenting with F-actin.

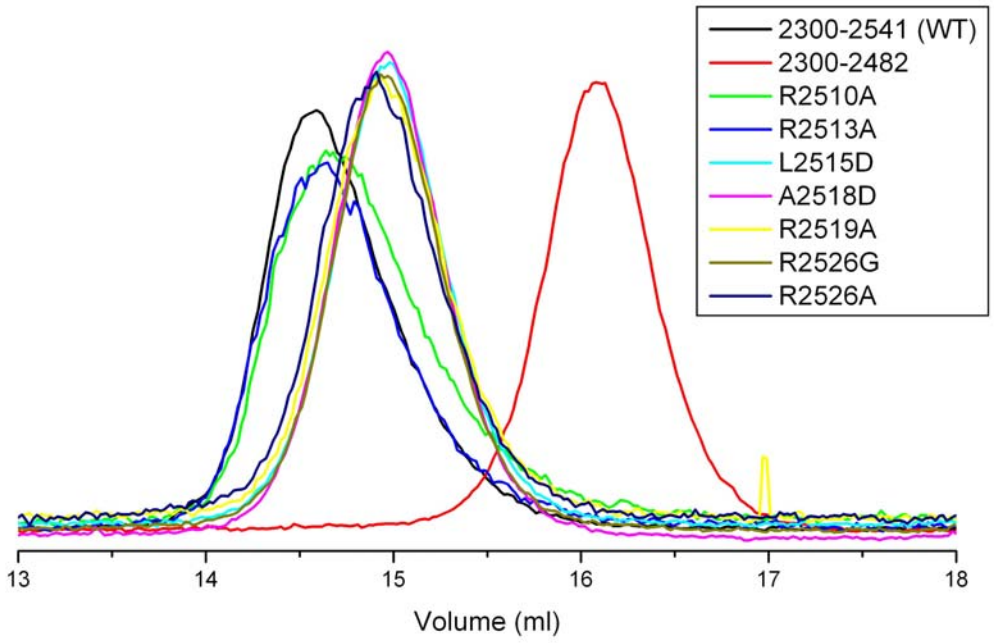

Figure S6 Gel filtration of talin THATCH domain polypeptides. Wild-type talin 2300-2541 elutes as a dimer (black line) in agreement with SAXS and NMR data. The construct lacking the dimerisation domain, residues 2300-2482, is monomeric (red line). Two of the mutants R2510A (green line) and R2513A (blue line) are also dimeric. However, NMR experiments indicate that five of the mutants analysed were monomeric, but they eluted ahead of the monomeric dimerisation domain deletion mutant (2300-2482) probably because the 60 residues at the C-terminus are unfolded.

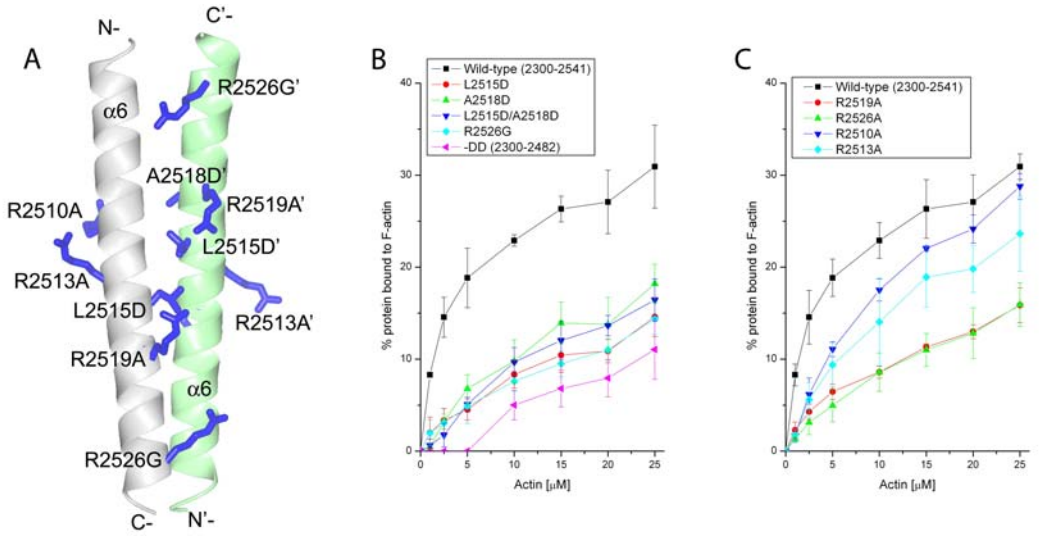

Figure S7 Dimerisation of the C-terminal actin-binding domain of talin is important for F-actin binding. (A) Ribbon diagram highlighting the residues in the dimerisation helix targeted by mutagenesis. All mutants showed reduced F-actin binding compared to wild-type. (B,C) Quantitative analysis of the effects of mutations on F-actin binding (means of three independent experiments). Bars represent standard deviations. Actin-binding was quantified by measuring the amount of the talin polypeptide cosedimenting with F-actin. (B) mutations that disrupt dimerisation. (C) Mutation of the invariant basic residues in the dimerisation domain.

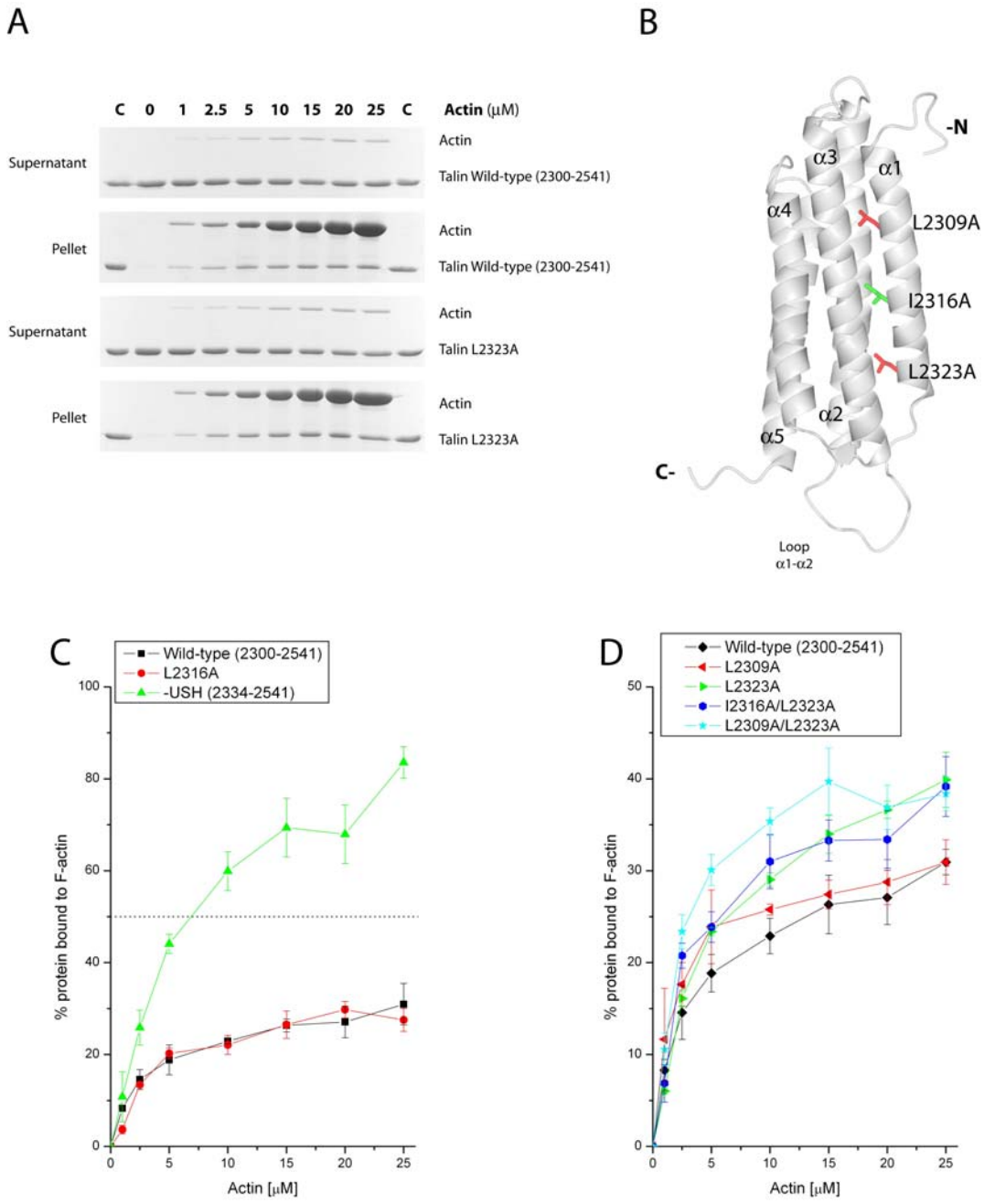

Figure S8 The C-terminal actin-binding domain of talin is regulated by the upstream helix (USH). (A) A representative F-actin co-sedimentation assay with talin wild-type (2300-2541) and a L2323A construct (4 μM) in the presence of increasing amounts of F-actin. The samples were centrifuged and the supernatants and pellet fractions were analysed by SDS-PAGE and stained with Coomassie blue. (B) Ribbon diagram highlighting the residues targeted by mutagenesis on the USH. Residues are colour coded according to the effects of the mutation on actin binding compared to wild-type: Red - increase in binding; Green - no change. (C,D) Actin-binding was quantified by measuring the amount of the talin polypeptide cosedimenting with F-actin.

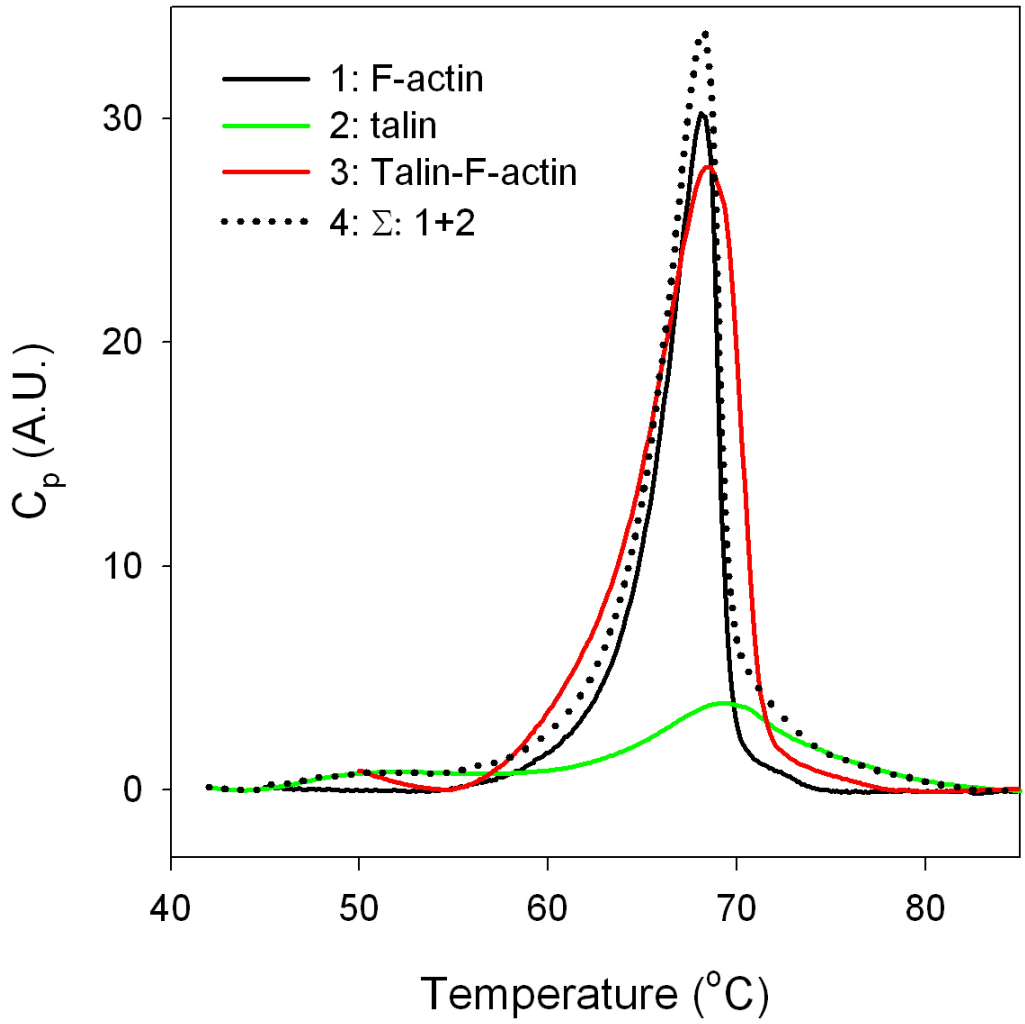

Figure S9 Characterisation of the talin 2334-2541 interaction with F-actin. Differential Scanning Calometry of F-actin, the C-terminal domain of talin and the complex of the two. These graphs indicate that both components are properly folded and that a complex is formed.

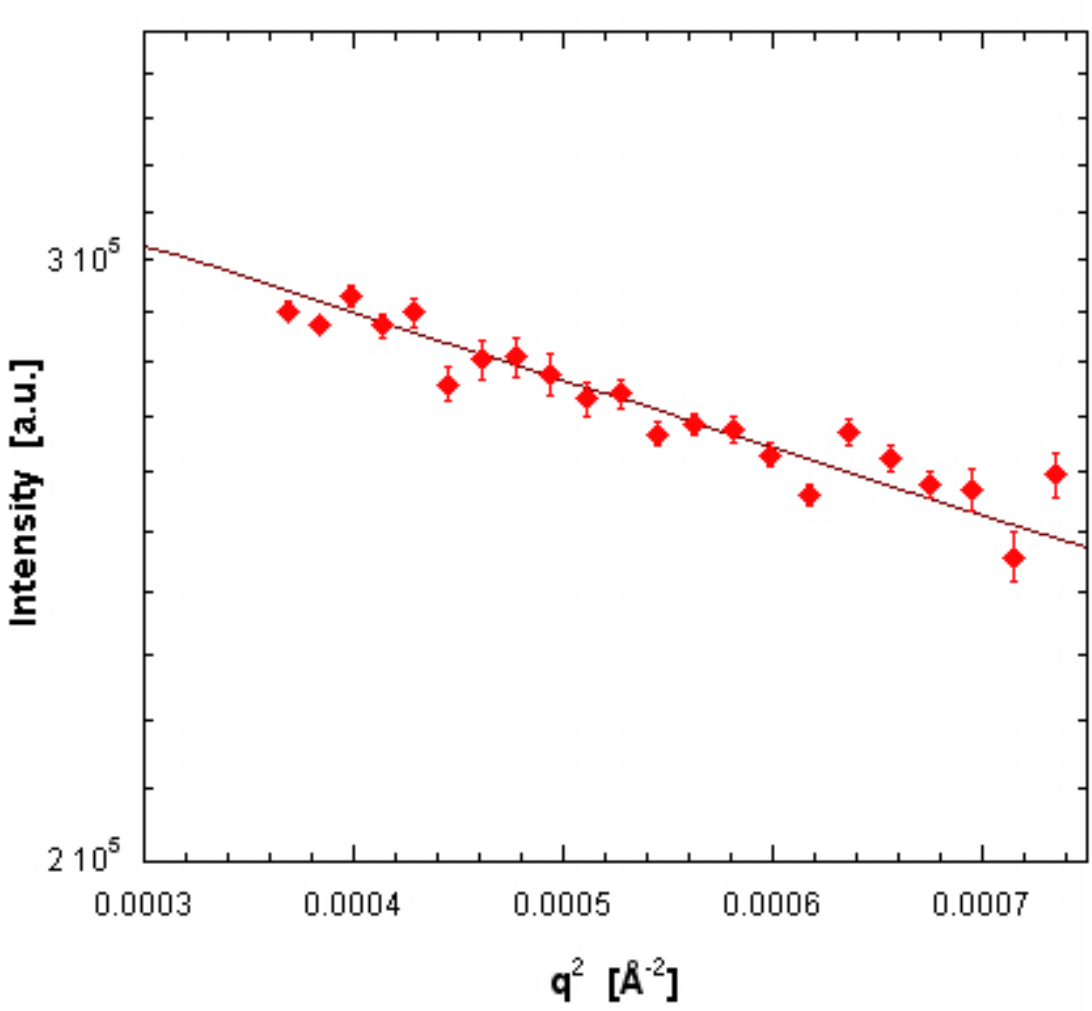

Figure S10 Small angle X-ray scattering on talin 2300-2541 - Guinier plot. No protein aggregation was detected and the linearity of the Guinier plot indicates that the protein solutions were homogeneous.

TABLES

Table SI Solution structure determination of talin 2300-2482.

Experimental restraints	
Unique/Ambiguous NOEs	3791/827
Intraresidue	1545/320
Sequential	832/155
Short range (1< [i – j] <5)	799/189
Long range ([i – j] >4)	615/163
φ/ψ dihedral angles[a]	290
Energies (Kcal mol^{-1})[b]	
Total	-7842 ± 96
Van Der Waals	-1602 ± 14
NOE	76 ± 12
RMS deviations[b]	
NOEs (Å) (no violations > 0.5 Å)	0.018 ± 0.001
Dihedral restraints (º) (no violations > 5º)	0.18 ± 0.06
Bonds (Å)	0.0032 ± 0.0001
Angles (º)	0.45 ± 0.01
Impropers (º)	1.28 ± 0.07
Ramachandran map analysis[c]	
Allowed regions	91.5%
Additional allowed regions	7.9%
Generously allowed regions	0.3%
Disallowed regions	0.4%
Pairwise rms difference (Å)[d]	
Residues 2301-2476	1.10 (1.55)
Secondary structure only, no loops	0.43 (0.83)

[a] From chemical shifts using Talos.

[b] Calculated in ARIA 1.2 for the 20 lowest energy structures refined in water.

[c] Obtained using PROCHECK-NMR.

[d] For backbone atoms; value for all heavy atoms in brackets.

TABLE SII Crystallographic analysis and refinement statistics on the talin dimerisation domain.

Data collection		
Space group	$P4_132$	
Cell dimensions	*a*,*b*,*c* = 98.82 Å α,β,γ = 90°	*a*,*b*,*c* = 98.56 Å α,β,γ = 90°
No. of molecules in a.u.	2	2
Data set	Native	Se-Methionine
Wavelength (Å)	1.07225	0.931
Resolution (Å)	30-2.2	50-2.3
Measured reflections	362276	157967
Unique reflections	8844	13705
Completeness (%)	94.9 (100.0)	100.0 (99.9)
R_{sym}	5.7 (53.1)	4.7 (44.3)
I/σI	51.71 (9.18)	32.15 (5.89)
Refinement statistics		
Resolution range (Å)	30-2.2 (2.257-2.2)	
Unique reflections (free)	8396 (442)	
R_{work} (%)	25.7 (24.2)	
R_{free} (%)	31.5 (31.2)	
Number of residues	65	
Number of solvent molecules	25	
Average B value ($Å^2$)	49.3	
Rmsd bond length (Å)	0.01	
Rmsd bond angles (Å)	1.092	
ESU based on R value (Å)	0.168	
ESU based on R_{free} value (Å)	0.184	

R_{sym} = Σ|I-<I>|ΣI, I is the observed intensity and <I> is the average intensity of the multiple observations of symmetry-related reflections. R = Σ||Fo|-|Fc||Σ|Fo|; R_{free} is calculated for a randomly-selected 5% of the reflections; R_{factor} is calculated for the remaining 95% of the reflections used in refinement. Values in brackets represent the outer resolution shell. ESU = Estimated Standard Uncertainties.

REFERENCES

Bakolitsa C, de Pereda JM, Bagshaw CR, Critchley DR, Liddington RC (1999) Crystal structure of the vinculin tail suggests a pathway for activation. *Cell* **99**: 603-613.

Breiter DR, Kanost MR, Benning MM, Wesenberg G, Law JH, Wells MA, Rayment I, Holden HM (1991) Molecular structure of an apolipoprotein determined at 2.5-A resolution. *Biochemistry* **30**: 603-608.

Brett TJ, Legendre-Guillemin V, McPherson PS, Fremont DH (2006) Structural definition of the F-actin-binding THATCH domain from HIP1R. *Nat Struct Mol Biol* **13**: 121-130.

Debye P (1915) Zerstreuung von Roentgenstrahlen. *Ann Phys* **46**: 809-823.

Emsley P, Cowtan K (2004) Coot: model-building tools for molecular graphics. *Acta Crystallogr D Biol Crystallogr* **60**: 2126-2132.

Guo DY, Blessing RH, Langs DA, Smith GD (1999) On 'globbicity' of low-resolution protein structures. *Acta Crystallogr D Biol Crystallogr* **55**: 230-237.

Herrmann T, Guntert P, Wuthrich K (2002) Protein NMR structure determination with automated NOE assignment using the new software CANDID and the torsion angle dynamics algorithm DYANA. *J Mol Biol* **319**: 209-227.

Kabsch W (1993) Automatic processing of rotation diffraction data from crystals of initially unknown symmetry and cell constants. *J. Appl. Cryst.* **26**: 795-800.

Linge JP, O'Donoghue SI, Nilges M (2001) Automated assignment of ambiguous nuclear overhauser effects with ARIA. *Methods Enzymol* **339**: 71-90.

Murshudov GN, Vagin AA, Dodson EJ (1997) Refinement of macromolecular structures by the maximum-likelihood method. *Acta Crystallogr D Biol Crystallogr* **53**: 240-255.

Papagrigoriou E, Gingras AR, Barsukov IL, Bate N, Fillingham IJ, Patel B, Frank R, Ziegler WH, Roberts GC, Critchley DR, Emsley J (2004) Activation of a vinculin-binding site in the talin rod involves rearrangement of a five-helix bundle. *Embo J* **23**: 2942-2951.

Senetar MA, Foster SJ, McCann RO (2004) Intrasteric inhibition mediates the interaction of the I/LWEQ module proteins Talin1, Talin2, Hip1, and Hip12 with actin. *Biochemistry* **43**: 15418-15428.

Terwilliger TC, Berendzen J (1999) Automated MAD and MIR structure solution. *Acta Crystallogr D Biol Crystallogr* **55**: 849-861.